

Relation between Aggregation Kinetics and the Structure of Kaolinite Aggregates

Marta Berka[†] and James A. Rice^{*}

Department of Chemistry and Biochemistry, South Dakota State University,
Brookings, South Dakota 57007

Received August 24, 2004. In Final Form: November 10, 2004

Dynamic and static light scattering were applied to the determination of the stability ratio and fractal dimension of kaolinite (KGa-2) at different kaolinite or/and electrolyte concentrations at pH 9.5. Dynamic light scattering was used to measure the kinetics of early stage aggregation to determine the stability ratio, W , as well as the cluster sizes which determine the fractal regime. Static light scattering was used to measure the fractal dimension, D_f . Results show that the two classes of “universality” (Lin et al. *Nature* **1989**, 339, 360) characterizing the diffusion- and reaction-limited regimes of cluster–cluster aggregation do apply to colloidal kaolinite as limit cases when $W \sim 1$ or $W > 100$, respectively. In the intermediate regime where $5 < W < 100$, the growth of the aggregate radius showed a power-law behavior similar to diffusion-limited cluster aggregation. For the intermediate aggregation regime, a scaling relation between fractal dimension and stability ratio, reflecting a continuous increase in particle packing density in the aggregate as the sticking probability of particles was reduced, was demonstrated.

Introduction

Aggregation involves the formation of assemblies of particles brought together by collisions and held in contact by surface forces.^{1,2} In many industrial operations, it is desirable to control the rate and extent of aggregation in order to control the morphology of the aggregates that are being formed. Particle aggregation and the compactness of the aggregates also play an important role in soil structure and in the transport of contaminants in aquatic environments.

Two distinct, limiting regimes of irreversible colloid aggregation have been identified.^{1,2} Diffusion-limited (or fast) colloid aggregation (DLCA) occurs when there is no repulsive force between the colloidal particles so that the aggregation rate is dependent solely on the time taken for particles (or clusters) to encounter each other by diffusion. The clusters themselves continue to diffuse, collide, and form larger clusters. In the regime of reaction-limited (or slow) cluster aggregation (RLCA), additional repulsive forces caused by electrostatic forces or steric hindrance prevent the particles from coagulating. Lin et al.^{3,4} have shown that each of these limiting regimes is associated with characteristic cluster growth kinetics and a cluster morphology that is independent of the chemical properties of a particular colloid system. A scaling analysis of light-scattering data can be used to compare aggregation behavior and provides convincing experimental evidence that the two aggregation regimes are indeed universal. Both cluster aggregation kinetics and the shape of cluster mass distribution are intrinsically related to the structure

of the clusters that ultimately result. Fractal structures can be quantified in terms of the fractal dimension.^{5–8} At high electrolyte concentration, coagulation in the DLCA regime typically leads to a low fractal dimension, D_f , of 1.7–1.8 reflecting the formation of loose, open particles. Reaction-limited cluster aggregation is evident in particles with a fractal dimension of 2.1–2.2. There is some evidence that below the critical coagulation concentration an intermediate regime exists between diffusion-limited and reaction-limited cluster aggregation that exhibits D_f values between 1.7 and 2.2 depending on the stability ratio, W , or sticking probability ($1/W$) of the system.^{9–12} The formation of structures more compact than expected for RLCA processes was explained in terms of particle restructuring^{13–15} which may be caused by reversibility¹⁶ or by surfactant molecules adsorbed on the particles.¹⁷

Experimental data relevant to the applicability of DLCA and RLCA to natural colloids can be found in the literature. For hematite clusters formed under DLCA or RLCA, the observed fractal dimensions were consistent with universality.^{18,19} For illite colloids which have a nonspherical morphology, the two universality classes were not applicable.¹⁰ For humic acid clusters or clusters in the

^{*} To whom correspondence should be addressed. E-mail: james.rice@sdsstate.edu.

[†] Permanent address: Department of Colloid and Environmental Chemistry, University of Debrecen, H-4010 Debrecen Egyetem tér 1, Hungary.

(1) Elimelech, M.; Gregory, J.; Jia, X.; Williams, R. A. *Particle deposition and aggregation: Measurement, modelling and simulation*; Butterworth-Heinemann Ltd.: Boston, 1995.

(2) Adachi, Y. *Adv. Colloid Interface Sci.* **1995**, *56*, 1–31.

(3) Lin, M. Y.; Lindsay, H. M.; Weitz, D. A.; Ball, R. C.; Klein, R.; Meakin, P. *Proc. R. Soc. London, Ser. A* **1989**, *423*, 71–87.

(4) Lin, M. Y.; Lindsay, H. M.; Weitz, D. A.; Ball, R. C.; Klein, R.; Meakin, P. *Nature* **1989**, *339*, 360–362.

(5) Meakin, P. *Adv. Colloid Interface Sci.* **1987**, *28*, 249–331.

(6) Martin, J. E. *Phys. Rev. A* **1987**, *36*, 3415–3426.

(7) Sorensen, C. M. *Aerosol Sci. Technol.* **2001**, *35*, 648–687.

(8) Bushell, G. C.; Yan, Y. D.; Woodfield, D.; Raper, J.; Amal, R. *J. Colloid Interface Sci.* **2002**, *95*, 1–50.

(9) Asnaghi, D.; Carpineti, M.; Sozzi, M. *Phys. Rev. A* **1992**, *45*, 1018–1023.

(10) Derrendinger, L.; Sposito, G. *J. Colloid Interface Sci.* **2000**, *222*, 1–11.

(11) Mellema, M.; van Opheusden, J. H. J.; van Vliet, T. *J. Chem. Phys.* **1999**, *111*, 6129–6135.

(12) Kim, A. Y.; Berg, J. C. *Langmuir* **2000**, *16*, 2101–2104.

(13) Aubert, C.; Cannell, D. S. *Phys. Rev. Lett.* **1986**, *56*, 738–741.

(14) Fernandez Nieves, A.; Fernandez Barbero, A.; Vincent, B.; de las Nieves, F. J. *Langmuir* **2001**, *17*, 1841–1846.

(15) Mellema, M.; Heesackers, J. W. M.; van Opheusden, J. H. J.; van Vliet, T. *Langmuir* **2000**, *16*, 6847–6854.

(16) Shih, W. Y.; Aksay, I. A.; Kikuchi, R. *Phys. Rev. A* **1987**, *36*, 5015–5019.

(17) Tirado Miranda, M.; Schmitt, A.; Callejas Fernandez, J.; Fernandez Barbero, A. *Langmuir* **1999**, *15*, 3437–3444.

(18) Chorover, J.; Zhang, J. W.; Amistadi, M. K.; Buffle, J. *Clays Clay Miner.* **1997**, *45*, 690–708.

(19) Zhang, J. W.; Buffle, J. *Colloids Surf., A* **1996**, *107*, 175–187.

presence of humic acids formed by RLCA, some results have been consistent with universality,^{20–22} and some results have shown significant departure from those required by universality.^{23–25} There is practical as well as fundamental interest in determining the relationship between aggregation kinetics and the structure.

In this paper, we studied the aggregation of dilute kaolinite suspensions. In particular, we have studied the average aggregate size as a function of time and the aggregate structure formed under high (above the critical coagulation concentration) and intermediate salt concentrations, $0.1 \text{ M} > [\text{NaCl}] > 0.01 \text{ M}$, to assess the universality of colloidal kaolinite's coagulation kinetics. In addition, the intermediate aggregation regime was examined to determine the quantitative relationship between aggregation kinetics and the aggregate structure by measuring the sticking probability in terms of the stability ratio, W , and the compactness of the aggregate in terms of the fractal dimension, D_f , of the clay.

Theoretical Background

The stability of a colloidal system can be characterized by the stability ratio, $W = k_{11,\text{fast}}/k_{11,\text{slow}}$, where $k_{11,\text{fast}}$ and $k_{11,\text{slow}}$ are the rate constants of doublet formation determined in early stages of diffusion-limited and reaction-limited coagulation, respectively. The stability ratio can be determined by measuring coagulation kinetics, or it can be calculated on the basis of Derjaguin–Landau–Verwey–Overbeek (DLVO) theory.^{26,27} The electrolyte concentration that separates DLCA from RLCA is referred to as the critical coagulation concentration, ccc , where $W = 1$. Considering the exact solution of the Smoluchowski equation^{1,28} for perikinetic irreversible aggregation with constant k_{ij} values for spherical colliding particles, the ratio of the initial particle number, N_0 , to the total particle number, $N_{\text{tot}}(t)$ after a t time of aggregation, is $N_0/N_{\text{tot}}(t) \sim (1 + t/t_a)$ where t_a is the characteristic Brownian aggregation time for doublet formation, $t_a = 1/(k_{11}N_0)$. The quantity $N_0/N_{\text{tot}}(t)$ is a measure of the average aggregate volume, which is proportional to the average number of primary particles (or monomers), N , in an aggregate; thus,

$$N \sim 1 + t/t_a \quad (1)$$

An important property of fractal aggregates is that their mass scales with their size raised to a power that is the fractal dimension.^{8,29}

$$N = k_0(R_{\text{ag}}/a)^{D_f} \quad (2)$$

where R_{ag} is a measure of the overall aggregate radius, a is the radius of a single particle, and k_0 is a propor-

tionality constant of order unity. From eq 1 and eq 2, the aggregation kinetics can be described as a simple power of the average radius of aggregates in terms of reduced time, t/t_a , according to eq 3:

$$R_{\text{ag}}(t) \sim (1 + t/t_a)^\alpha \quad (3)$$

where the exponent α is a constant in the range $\sim 0.2–0.6$ depending on the sticking probability and volume fraction. For diffusion-limited aggregation, $\alpha = z/D_f$ where z is approximately 1.^{3,30} The determination of the fractal dimension can be accomplished with a log–log plot of the aggregation size as a function of time and yields a fractal dimension with the value of $D_f \sim 1.75–1.8$. No equivalent expression relating the radius of aggregates to the fractal dimension has been derived for RLCA aggregates. In this case, an exponential increase of the average cluster sizes for a substantial range of aggregation times was described using eq 4.³

$$R_{\text{ag}}(t) \sim e^{\alpha t} \quad (4)$$

The fractal dimension is readily determined by static light scattering, SLS,^{7,8,29} since the structure factor, $S(q)$, is given by

$$S(q) \sim q^{-D_f} \quad \text{if } R_{\text{ag}}^{-1} < q < a^{-1} \quad (5)$$

where the scattering vector, q , is given by $q = (4\pi\lambda) \sin(\theta/2)$, λ is the wavelength of the light in the medium, and θ is the scattering angle. The structure factor is proportional to the average scattered intensity, $I(q)$, which can be readily measured experimentally using SLS. A simple way to determine the mass fractal dimension is from the slope of the linear region of a $\log I(q)$ vs $\log q$ plot instead of the $\log S(q)$ versus $\log q$ plot for dilute dispersions of aggregates formed by small particles in the fractal regime $R_{\text{ag}}^{-1} < q < a^{-1}$. In view of the fact that a radius is ill-defined for a colloidal aggregate given its indefinite perimeter, the radius of gyration, R_g , of the aggregate has been generally taken as R_{ag} . In a fractal analysis, the Guinier regime ($qR_g < 1$) is first evaluated to give R_g . The power law $S(q) \sim q^{-D_f}$ behavior begins ($qR_{\text{ag}} > 1$) immediately after the Guinier regime, but the scaling cannot address the crossover region $qR_g \sim 1$. For fractal aggregates, the hydrodynamic radius, R_h , is also proportional to the physical extent of the aggregate; hence it also can be used for the determination of the fractal regime. The replacement of R_{ag} with R_h is useful because determination of the fractal dimension becomes possible for larger particles using simultaneous dynamic and static light scattering. In this research, the fractal regime was defined where $qR_h > 2.5$ and $q^{-1} < a^{-1}$. The power-law regime yields the fractal dimension through its slope.⁷

The universality of coagulation in both regimes was examined through the kinetics of aggregation by eq 3 and eq 4 as well. The fractal dimensions, D_f , were determined from the static light scattering measurements with eq 5 and from the hydrodynamic radius vs time function (eq 3) in the case of DLCA.

Experimental Section

Materials. The kaolinite (KGa-2) used in this study was obtained from the Source Clay Minerals Repository of The Clay Minerals Society. The kaolinite was mixed with deionized water (NANOpure Barnstead) and the suspension pH was increased

(20) Ren, S. Z.; Tombacz, E.; Rice, J. A. *Phys. Rev. E* **1996**, *53*, 2980–2983.

(21) Tombacz, E.; Rice, J. A.; Ren, S. Z. *ACH—Models Chem.* **1997**, *134*, 877–888.

(22) Rice, J. A.; Tombacz, E.; Malekani, K. *Geoderma* **1999**, *88*, 251–264.

(23) Elfarissi, F.; Pefferkorn, E. *J. Colloid Interface Sci.* **2000**, *221*, 64–74.

(24) Senesi, N.; Rizzi, F. R.; Dellino, P.; Acquafredda, P. *Soil Sci. Soc. Am. J.* **1996**, *60*, 1773–1780.

(25) Senesi, N.; Rizzi, F. R.; Dellino, P.; Acquafredda, P. *Colloids Surf., A* **1997**, *127*, 57–68.

(26) Derjaguin, B. V.; Landau, L. *Acta Physicochim. U.S.S.R.* **1941**, *14*, 633–662.

(27) Verwey, E. J. W.; Overbeek, J. T. G. *Theory of the Stability of Lyophobic Colloids*; Elsevier: Amsterdam, 1948.

(28) Smoluchowski, M. Z. *Phys. Chem.* **1917**, *92*, 129–168.

(29) Sorensen, C. M. *Scattering and absorption of light by particles and aggregates*, 2nd ed.; Birdi, K. S., Ed.; CRC Press: New York, 2003; pp 623–652.

(30) Lach-hab, M.; Gonzalez, A. E.; BlaistenBarojas, E. *Phys. Rev. E* **1996**, *54*, 5456–5462.

to $\text{pH } 9.5 \pm 0.1$ by NaOH addition resulting in complete dispersion. The suspension was kept under a blanket of nitrogen throughout the experiment. After several intensive sonication and centrifugation steps, a size fraction with a radius of $< 0.2 \mu\text{m}$ was separated and collected. The pH and the electrolyte concentration of the suspension were adjusted to $\text{pH} \sim 3$ with HCl and to $\sim 1 \text{ M}$ with NaCl, and the sample was allowed to equilibrate overnight. The precipitated clay was washed repeatedly with 1 M NaCl. The Na-saturated kaolinite was washed free of excess salt with deionized water and freeze-dried. Stock solutions ($0.05\text{--}0.1 \text{ mg cm}^{-3}$) were prepared by intensive sonication at $\text{pH } 9.5$ where kaolinite forms a stable dispersion without dissolution before the aggregation experiment. The z -average radius of gyration was determined to be $R_g = 97 (\pm 1\%) \text{ nm}$. The spherical equivalent hydrodynamic radius in a 0.01 mg/mL kaolinite solution was $R_h \sim 100 \pm 5 \text{ nm}$ determined at 90° calculated by first cumulant. N_0 was determined for kaolinite as reported earlier.³¹ Light scattering experiments were conducted with dilute kaolinite suspensions containing $0.005\text{--}0.05 \text{ mg/mL}$ or 6.5×10^{14} to 6.5×10^{15} particles m^{-3} kaolinite.

Instrumentation. Dynamic and static light scattering experiments were performed on an ALV 5000 laser light scattering apparatus with standard pinhole optics, an ALV-Goniometer system, and an ALV-5000E Multiple Tau Digital Correlator. An argon ion laser (Lexel Laser model 95) operated at a wavelength of 514.5 nm was employed as the light source. The stability of the laser power was controlled by four monitoring diodes. The autocorrelation functions of the dynamic light scattering experiment were generally performed over a 10 s interval and fitted with a nonlinear least-squares fit using a first-order cumulant method. For fractal determinations, static light scattering data (and simultaneously, the hydrodynamic radius) were measured over scattering angles of $12^\circ\text{--}45^\circ$ which corresponds to the range $0.0034 \text{ nm}^{-1} < q < 0.0122 \text{ nm}^{-1}$.

Transmission electron micrographs of clusters were acquired with a Hitachi H-7000 FA transmission electron microscope (TEM). A TEM sample was prepared by placing $5 \mu\text{L}$ of a clay suspension on a silicon-oxide-coated copper grid on a filter paper that instantly absorbed the solution. The grid with some particles on its surface was allowed to air-dry and placed in the TEM. Silicon oxide films create some background texture, but this does not interfere with the particle images.

Methods. The temperature during all measurements was $25.0 \pm 0.1^\circ \text{C}$. The experiments began with sonication, pH adjustment, and determination of the size distribution of the particles in the stock solution. These preparation steps are the determinative factor for experiment reproducibility. Samples were prepared from a given volume of stock solution and an appropriate volume of water or solution of NaCl filtered through a $0.2 \mu\text{m}$ membrane filter into 10 mm diameter light scattering vials. In the coagulation experiments, 1.8 mL of electrolyte solution was poured into 0.2 mL of stock solution and poured back and sealed; this point was considered to be time zero as the beginning of coagulation. Since the volume of the salt solution is much larger than that of the clay suspension, the mixing action produced by pouring the salt solution into the sol and pouring it back into the first vial leads to sufficiently fast homogenization of the system without any further mechanical mixing. For kinetic measurements, the hydrodynamic radius and the scattered intensity were monitored as a function of time at a given scattering angle until the radius of aggregates was large enough ($qR_h > 1$). The scattered intensity angular function was then determined, from which the fractal dimension was calculated. The stability ratio (or k_{11} and t_a) and the corresponding fractal dimension were calculated from the same coagulation experiment.

Results and Discussion

Coagulation Kinetics. Interpretation of the DLS data is complex since it depends on less universal aspects of the aggregates such as flexibility and polydispersity of the clusters. All of the dynamic processes of the aggregates (translational diffusion, rotational diffusion, and internal modes) contribute to some degree to the correlation

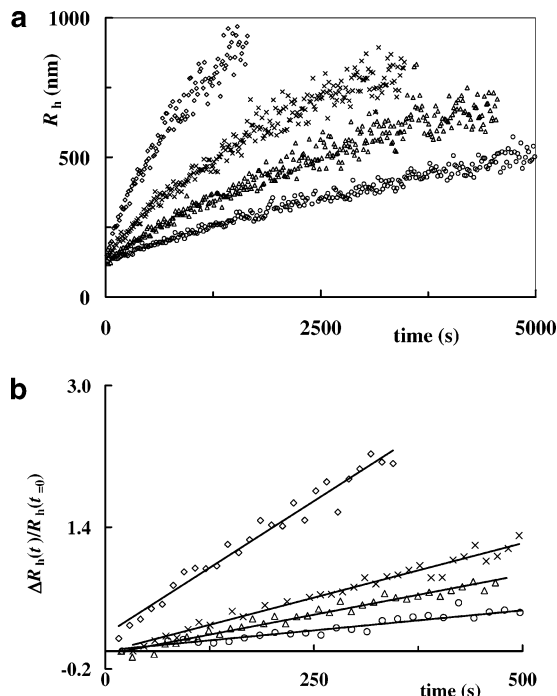


Figure 1. (a) Hydrodynamic radius $R_h(t)$ and (b) initial change of the normalized hydrodynamic radius, $(R_h(t) - R_h(0))/R_h(0)$ as a function of time measured in DLCA. Concentration of kaolinite, N_0 , particles m^{-3} : (\diamond) 6.56×10^{15} , (\times) 2.63×10^{15} , (\triangle) 1.31×10^{15} , (\circ) 6.56×10^{14} , $\text{pH } 9.5$; $[\text{NaCl}] = 0.5 \text{ M}$; $\log W = 0$. Lines indicate the fitted slopes.

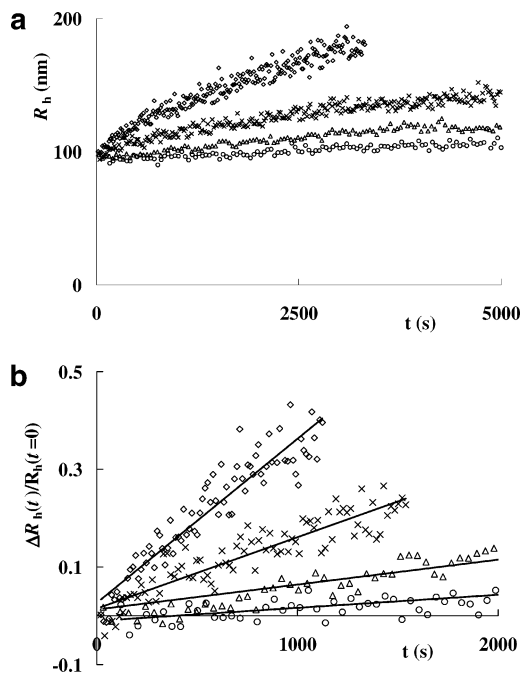


Figure 2. (a) Hydrodynamic radius $R_h(t)$ and (b) initial change of the normalized hydrodynamic radius, $(R_h(t) - R_h(0))/R_h(0)$ as a function of time in RLCA. Concentration of kaolinite, N_0 , particles m^{-3} : (\diamond) 6.56×10^{15} , (\times) 2.63×10^{15} , (\triangle) 1.31×10^{15} , (\circ) 6.56×10^{14} , $\text{pH } 9.5$; $[\text{NaCl}] = 0.05 \text{ M}$; $\log W \sim 1.35$. Lines indicate the fitted slopes.

function.⁶ Thus, the measured hydrodynamic radius is best viewed as an apparent average radius. The coagulation rate constant was determined in the early stages of coagulation where $t \leq (2\text{--}3)t_a$ by dynamic light scattering at 90° or 30° . From the data in Figure 1 and Figure 2, it can be seen that the coagulation rates were proportional

(31) Berka, M.; Rice, J. A. *Langmuir* **2004**, *20*, 6152–6157.

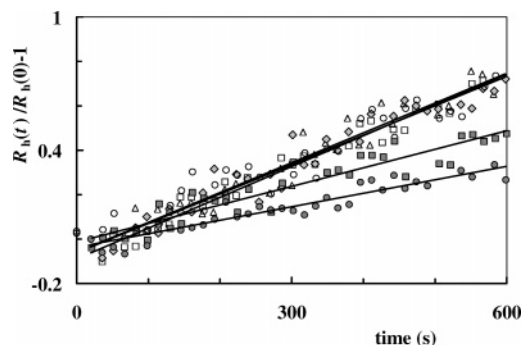


Figure 3. Initial change of the normalized hydrodynamic radius, $(R_h(t) - R_h(0))/R_h(0)$ as a function of time measured by DLS at an angle of 30° at different concentrations of NaCl: (Δ) 0.35 M, (\square) 0.2 M, (\diamond) 0.15 M, (\circ) 0.1 M, (\blacksquare) 0.075 M, (\bullet) 0.05 M. $N_0 = 1.3 \times 10^{15}$ particles m^{-3} ; pH 9.5. Lines indicate the fitted slopes.

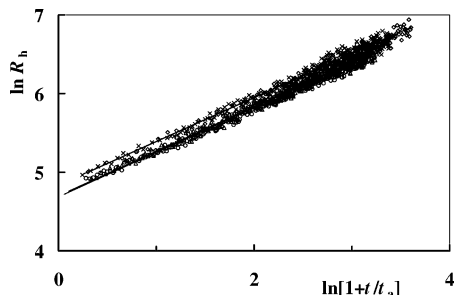


Figure 4. Master curves for DLCA. Power-law growth of the average hydrodynamic radius for data shown in Figure 1. Lines indicate the fitted slopes.

to the concentration of kaolinite in both the DLCA (Figure 1) and RLCA (Figure 2) regimes. Consequently, the ratio of the slope of the initial change of the hydrodynamic radius and initial concentration of kaolinite suspension (slope/ N_0) was constant within 10%. With increasing electrolyte concentration in the RLCA regime, the slopes of the lines increase up to an electrolyte concentration of ~ 0.1 M NaCl (Figure 3). The critical coagulation concentration which separates the two regimes was found to be $\text{ccc} = 0.09$ mol dm^{-3} from the stability plot.³¹

According to theory, the universality of the DLCA and RLCA regimes is characterized by distinctly different growth kinetics. Evaluating the data in Figure 1 with eq 3 produces a power-law growth in the average cluster sizes (Figure 4). It was found that the data from different concentrations plotted as a function of the reduced time, t/t_a , were collapsed into one master curve, with a slope of the line $\alpha = 0.561 \pm 0.005$. That means that the compactness of the clusters has not changed with the concentration of kaolinite over the range examined. The fractal dimension calculated from the slopes is $D_f = 1.783 \pm 0.005$. It is important to note that this result has been obtained for a low-volume-fraction regime and in a more concentrated regime the compactness of the clusters may change with the concentration, and hence the fractal dimension should change, which may be important in industrial applications.

An exponential increase of mean cluster sizes with time has been described for RLCA.^{3,4} We found straight lines in the $\ln R_h$ vs t plots only in the case of very slow aggregation, for example, in the case of the bottom curves in Figure 5a and in Figure 6a, where $N_0 < 1.3 \times 10^{15}$ particles m^{-3} and $[\text{NaCl}] \leq 0.06$ M. The shapes of the kinetic curves are influenced not only by the sticking probability of the two particles ($1/W$) but by the time

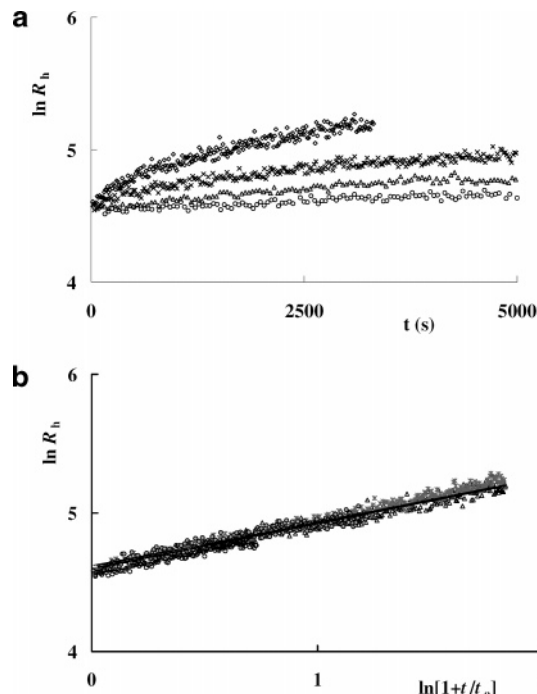


Figure 5. Growth of the average hydrodynamic radius in RLCA. Concentration of kaolinite, N_0 , particles m^{-3} : (\diamond) 6.5×10^{15} , (\times) 2.6×10^{15} , (Δ) 1.3×10^{15} , (\circ) 6.5×10^{14} , pH 9.5; $[\text{NaCl}] = 0.05$ M. Panel a represents $\log R_h$ as a function of time. Panel b represents the master curve for RLCA (\log – \log plot of R_h as a function of the reduced time).

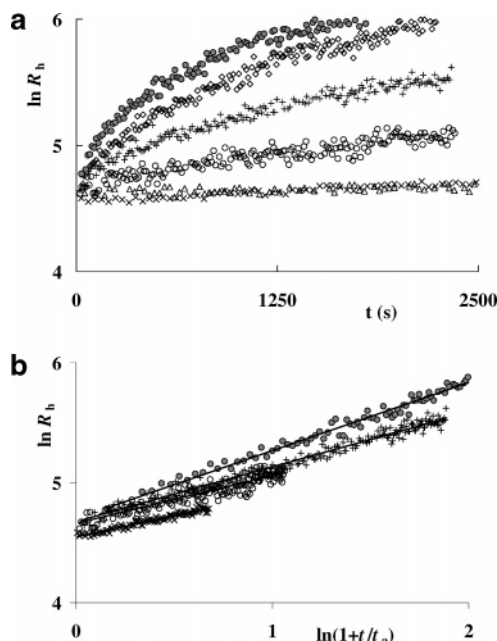


Figure 6. The logarithmic average hydrodynamic radius versus (a) time and (b) the logarithm of the reduced time. Concentration of electrolyte: (\bullet) 0.5 M; (\diamond) 0.125 M; ($+$) 0.1 M; (\circ) 0.07 M; (Δ) 0.06 M; (\times) 0.05 M. $N_0 = 1.3 \times 10^{15}$ particles m^{-3} ; pH 9.5. Lines indicate the fitted slopes.

between collisions as well. Plotting in terms of reduced time, the \log – \log plots of the data give straight lines and collapse onto a master curve for different sol concentrations in Figure 5b similar to Figure 4. The slopes of the lines in Figure 5b were determined as 0.32 ± 0.01 at an electrolyte concentration of 0.05 M. The \log – \log plot of the function R_h vs $[1 + t/t_a]$ still shows a linear relationship for different electrolyte concentrations (Figure 6b). In other

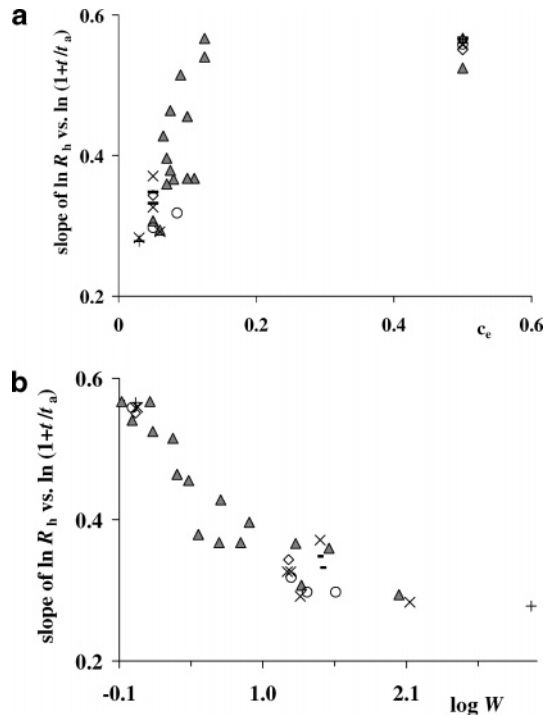


Figure 7. Power-law exponent as a function of (a) the concentration of electrolyte and (b) the measured stability of the sol. Concentrations of kaolinite, N_0 , particles m^{-3} : (-) 6.5×10^{14} , (\blacktriangle) 1.3×10^{15} , (\circ) 2.6×10^{15} , (+) 3.9×10^{15} , (\diamond) 5.3×10^{15} , (\times) 6.5×10^{15} .

words, the power-law growth of the hydrodynamic radius remains valid for the intermediate regime too. To determine where an exponential growth starts instead of the power-law behavior, linear regression of the logarithmic radius versus time and versus the logarithm of the reduced time was compared.

In the intermediate regime between DLCA and RLCA, the power-law regime exhibits an exponent decreasing from $\alpha \sim 0.6$ to $\alpha \sim 0.3$ with decreasing electrolyte concentration and it decreases with increase of the stability of the sol as Figure 7 shows.

The time dependence of the aggregate radius shows that the kinetics is similar in the intermediate regime to that observed for DLCA, and the power-law exponent depends on the electrolyte concentration. This is not surprising in the case of the early stage of the coagulation ($t/t_a < 6$) when the $\ln R_h$ vs $\ln(1 + t/t_a)$ and the $\ln R_h$ vs t functions run very close to each other. The crossover to exponential behavior is very slow at small values of qR . The exponential growth for slow coagulation is expected at larger times and larger qR values.⁶ We found that this behavior was attained when $W \sim 100$ or a sticking probability of 0.01.

Fractal Dimension. The fractal dimension was calculated from the linear portion of the $\log I(q)$ vs $\log q$ curve where $qR_h > 2.5$; thus the fractal regime covers roughly half a decade. In the case of DLCA, aggregation takes place so rapidly that the $qR_{ag} \sim 1$ region quickly falls outside the observation range (Figure 8a,b). The $\log I(q)$ vs $\log q$ and $\log I(q)$ vs $\log qR_{ag}$ curves show straight lines, and their slopes are essentially constant 25 min after the start of aggregation. The linear regime begins at $\log qR_{ag} > 0.3$ and the fractal regime changes as the aggregate size increases with coagulation time (Figure 8b). The average radius of the aggregate was larger than 500 nm; hence the number of monomers (N) in the cluster was larger than 15. The fractal dimension was $1.69 \pm$

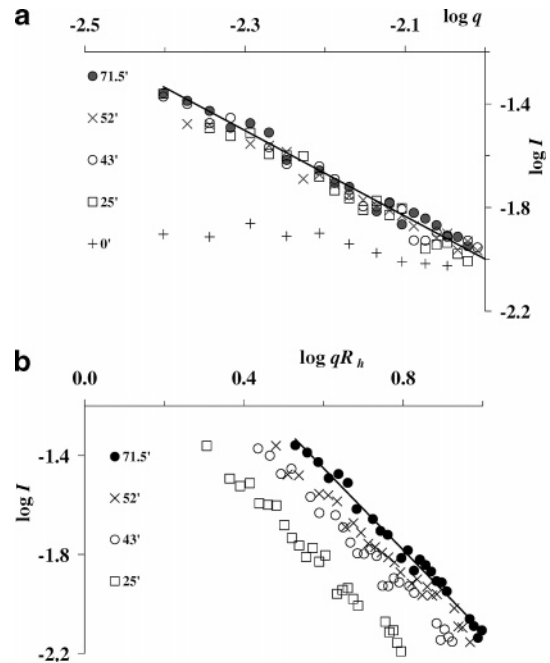


Figure 8. Static light scattering curves in DLCA at various times during coagulation. (+) Before coagulation, $R_h \sim 100$ nm. Coagulation time: (\square) 25 min, $R_h \sim 500$ nm; (\circ) 43 min, $R_h \sim 688$ nm; (\times) 52 min, $R_h \sim 762$ nm; (\bullet) 71.5 min, $R_h \sim 853$ nm. The line shows the slope of -1.67 . $N_0 = 1.3 \times 10^{15}$ particles m^{-3} ; [NaCl] = 0.9 M.

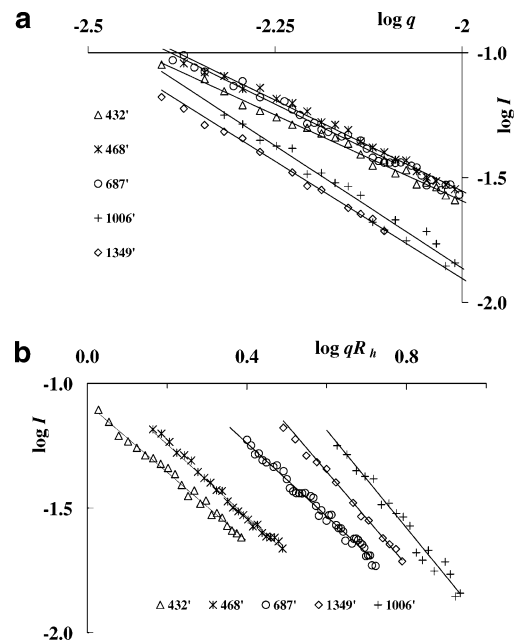


Figure 9. Static light scattering curves in RLCA at various times during coagulation. Coagulation time: (\triangle) 432 min, $R_h \sim 230$ nm; (\times) 468 min, $R_h \sim 260$ nm; (\circ) 687 min, $R_h \sim 420$ nm, (+) 1006 min, $R_h \sim 880$ nm; (\diamond) 1349 min, $R_h \sim 780$ nm. $D_f \sim 2.0$; $N_0 = 6.56 \times 10^{15}$ particles m^{-3} ; [NaCl] = 0.03 M.

0.07 determined from the slope of the linear part of the curves which is smaller than that measured by dynamic light scattering (DLS) ($D_f = 1.783 \pm 0.005$).

For the intermediate regime, the fractal dimension increased with decreasing electrolyte concentration up to a value of ~ 2.1 which is typical of RLCA. Though the slope changes over the course of the reaction (Figure 9 and Figure 10), the fractal dimension should be invariant. When the average number of monomers (N) in the cluster achieves about $N > 15$ ($R_h > 400$ nm), the linear region

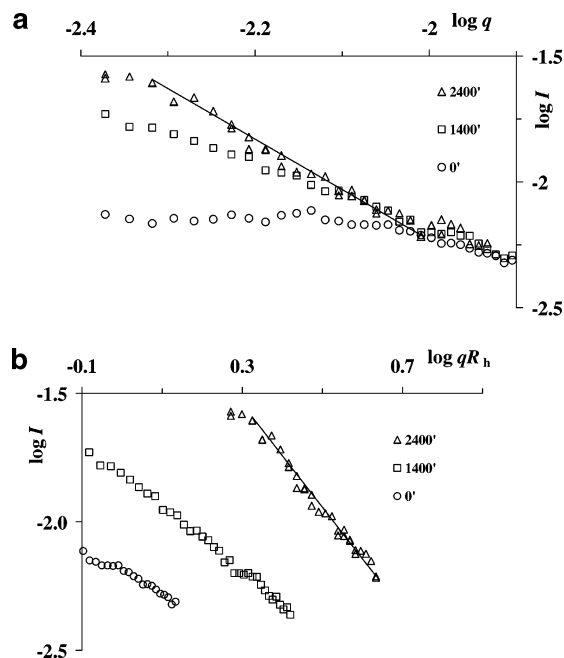


Figure 10. Static light scattering curves in RLCA at various times during coagulation. Coagulation time: (○) 0 min, $R_h \sim 100$ nm; (□) 1400 min, $R_h \sim 210$ nm; (△) 2400 min, $R_h \sim 440$ nm. $D_f \sim 2.0$; $N_0 = 1.3 \times 10^{15}$ particles m^{-3} ; [NaCl] = 0.02 M.

of the $\log I(q)$ vs $\log q$ plot is well-defined and the slope does not change (Figure 9 and Figure 10).

In the case of very slow aggregation, the effect of sedimentation can be seen at longer times because the curves taken from the same experiment but at different times do not collapse onto the same asymptotic line but, instead, decrease because of the settling of large aggregates in the sample (for example, the curves at 1006 and 1349 min in Figure 9). It was found that when the aggregates had already formed fractal structures the value of the slope of the $\log I(q)$ vs $\log q$ curve was not sensitive to the initial sedimentation. However, if the average aggregate size was still not large enough to show a fractal character, then the particle fractal dimension could not be determined. In that case, the initial sol concentration was increased to a sufficiently high value so that the largest clusters did not sediment during the measurement.

There are several references in the literature to the effects of ionic strength on fractal structures^{17,18,25,32,33} and some discussing the relationship between the fractal dimension and stability ratio.^{11,12,34} Kim and Berg¹² determined a relationship of $D_f = 0.37(\log W) + 1.45$ for the measured fractal dimension and the calculated stability ratio for polystyrene latex particles. Mellema et al.¹¹ found from simulations that the correlation of the relationship of $D_f \sim \log W$ strongly depends on the volume fraction and at a low volume fraction it achieved a steady state of $D_f \sim 2.1$ at $W > 5$. Norgren et al.³⁴ published an empirical equation for the measured (not calculated) $D_f \sim \log W$ function for aggregation of lignin derivatives as $D_f = 0.32(\log W) + 2.04$. The relationship we have determined for kaolinite, $D_f = 0.17(\log W) + 1.67$, agrees well with the predicted one (Figure 11). The agreement indicates that Smoluchowski's conditions are probably met

(32) Burns, J. L.; Yan, Y. D.; Jameson, G. J.; Biggs, S. *Langmuir* **1997**, *13*, 6413–6420.

(33) Ikeda, S.; Foegeding, E. A.; Hagiwara, T. *Langmuir* **1999**, *15*, 8584–8589.

(34) Norgren, M.; Edlund, H.; Wagberg, L. *Langmuir* **2002**, *18*, 2859–2865.

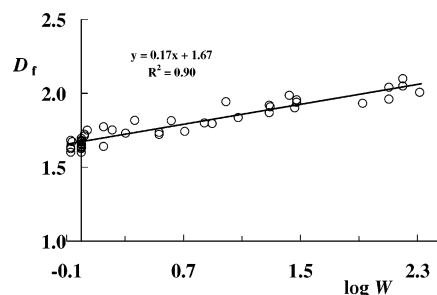


Figure 11. Fractal dimension D_f as a function of the stability ratio, W .

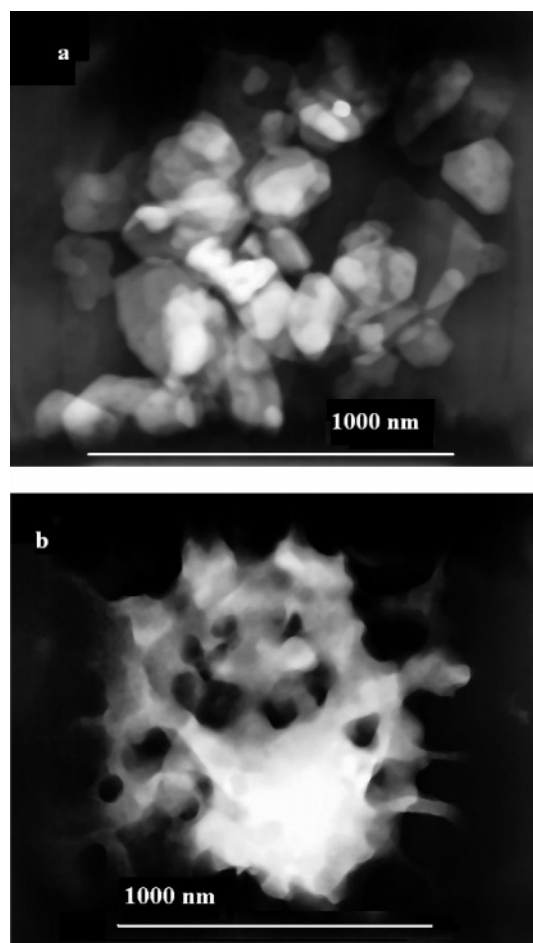


Figure 12. Transmission electron micrographs of clay aggregates formed during (a) DLCA and (b) RLCA. N_0 , particles m^{-3} : (a) 1.3×10^{15} , (b) 6.5×10^{15} . [NaCl]: (a) 0.1 M, (b) 0.01 M. pH 9.5; coagulation time, 2 days.

because the early-time kinetics controls the aggregate structure formed during longer aggregation time periods.

The transmission electron micrographs of two aggregates of similar size formed during DLCA and RLCA are shown in Figure 12. In both cases the particles attach in a face-to-face orientation at pH 9.5. The aggregate formed in DLCA (Figure 12a) shows a looser, less compact structure than the aggregate formed in RLCA (Figure 12b). In RLCA, the edge of the cluster is loosely associated but the interior is so dense packed that it is difficult to distinguish the primary particles. This observation agrees with conclusions obtained from the fractal dimensions.

Conclusion

The aggregation of colloidal kaolinite particles has been experimentally investigated using simultaneous dynamic

and static light scattering. The interaction between particles was controlled through the addition of NaCl. Aggregation processes above the critical coagulation concentration (DLCA) and below (RLCA) were examined. Attention has been focused on the early-stage aggregation kinetics as well as the structure of the clusters formed during the process. Our results show that the two “universality” classes proposed by Lin et al.^{3,4} to characterize the diffusion- and reaction-limited regimes of cluster–cluster aggregation do apply to colloidal kaolinite. In the DLCA regime, the results were in general agreement with those required by universality: the fractal dimension determined by SLS was $D_f \sim 1.69$ and the cluster sizes determined by DLS increased according to a power law. The exponent was found to be $\alpha = 0.56$; hence $D_f \sim 1.78$.

The universality of RLCA was confirmed through the exponential growth of the average aggregate, and $D_f \sim 2.1$ when the stability ratio was $W \geq 100$. In the intermediate regime where $5 < W < 100$, the aggregate radius varies according to a power law in a fashion similar to DLCA. The exponent, that is, the slope of the plot of $\ln R_h$ vs $\ln(1 + t/t_a)$, decreased with decreasing electrolyte concentration and increasing stability ratio from 0.56 to

0.28. In the case of RLCA, the aggregation time may be so long and the cluster distribution so broad that precautions must be taken to avoid differential settling due to gravity. The results presented clearly demonstrate the consistency of experiments with natural colloids and theory without reliance on adjustable parameters. DLCA is the result of pure diffusion with a sticking probability equal to 1; RLCA behavior is the result of very slow aggregation with a sticking probability of < 0.01 in a very dilute sol. The crossover (so-called intermediate regime) between the DLCA and RLCA is slow. In the intermediate regime, the fractal dimension increased linearly between its two characteristic values with increasing stability ratio. This means that the compactness of the clay aggregates can be controlled through the electrolyte concentration during coagulation.

Acknowledgment. This work was supported by a grant from the South Dakota Water Resources Research Institute, by National Science Foundation/EPSCoR Grant No. EPS-0091948, and by the State of South Dakota.

LA0478853